

Particle removal challenges with EUV patterned masks for the sub-22 nm HP node

Abbas Rastegar^{*a}, Sean Eichenlaub^a, Arun John Kadaksham^a, Byunghoon Lee^a, Matt House^a,
Sungmin Huh^a, Brian Cha^a, Henry Yun^a, Iacopo Mochi^b, Kenneth Goldberg^b

^aSEMATECH, 257 Fuller Road, Suite 2200 Albany, NY 12203

^b Center for X-Ray Optics, Lawrence Berkley National Laboratory, Berkley CA 94720

*Abbas.Rastegar@sematech.org

ABSTRACT

The particle removal efficiency (PRE) of cleaning processes diminishes whenever the minimum defect size for a specific technology node becomes smaller. For the sub-22 nm half-pitch (HP) node, it was demonstrated that exposure to high power megasonic up to 200 W/cm² did not damage 60 nm wide TaBN absorber lines corresponding to the 16 nm HP node on wafer. An ammonium hydroxide mixture and megasonics removes ≥ 50 nm SiO₂ particles with a very high PRE. A sulfuric acid hydrogen peroxide mixture (SPM) in addition to ammonium hydroxide mixture (APM) and megasonic is required to remove ≥ 28 nm SiO₂ particles with a high PRE. Time-of-flight secondary ion mass spectroscopy (TOF-SIMS) studies show that the presence of O₂ during a vacuum ultraviolet (VUV) ($\lambda=172$ nm) surface conditioning step will result in both surface oxidation and Ru removal, which drastically reduce extreme ultraviolet (EUV) mask life time under multiple cleanings. New EUV mask cleaning processes show negligible or no EUV reflectivity loss and no increase in surface roughness after up to 15 cleaning cycles. Reviewing of defect with a high current density scanning electron microscope (SEM) drastically reduces PRE and deforms SiO₂ particles. 28 nm SiO₂ particles on EUV masks age very fast and will deform over time. Care must be taken when reviewing EUV mask defects by SEM. Potentially new particles should be identified to calibrate short wavelength inspection tools. Based on actinic image review, 50 nm SiO₂ particles on top of the EUV mask will be printed on the wafer.

Keywords: EUVL, Mask Defects, sub-20 nm defects cleaning, defect printability, SEM damage, Ru oxidation

1. INTRODUCTION

Extreme ultraviolet lithography (EUVL) is the technology of choice for the sub-22 nm half-pitch node among major semiconductor manufacturers. In contrast to conventional optical masks, EUV patterned masks work in reflective mode. These masks introduce new materials and surfaces that pose challenges to particle adhesion and cleaning. The process of fabricating an EUV mask includes deposition of 40 to 50 pairs of MoSi bilayers on top of an extra smooth low thermal expansion material (LTEM) substrate. Typically, the MoSi multilayer (ML) is capped by a 2.5 nm Ru layer. An absorber stack composed of Ta, N, B, and O, 50 to 70 nm thick, is coated on top of the capping layer. EUV masks are built by patterning this absorber stack. Currently, an anti-reflecting coating (ARC) layer is deposited on top of the absorber stack. Material for the ARC layer is chosen so that its reflectivity is maximized at the wavelength of patterned mask inspection tools. For example, ~13 nm thick SiON is optimized for $\lambda=257$ nm, and ~7 nm thick HfO with is optimized for $\lambda=193$ nm in newer generations of inspection tools. (See Fig. 1.)

Therefore, in an EUV mask, surfaces are exposed to chemicals, including Si_xO_yN_z, Ta_xN_y, Ta_xN_yB_zO_w, Ru, Si, Mo, MoSi multilayers, Ti-doped SiO₂ (LTEM), Cr_xN_y, TiO₂, HfO, and Cr. Depending on the blank supplier or patterning process, some EUV masks may include a combination of above materials.

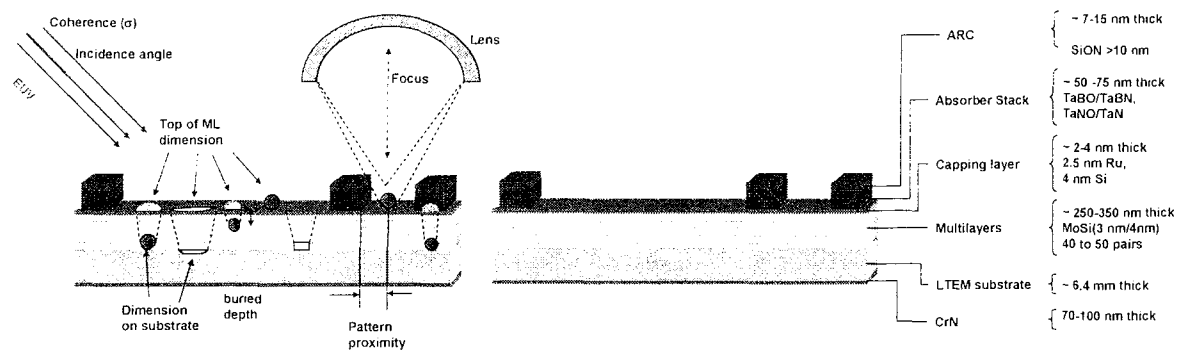


Figure 1- Structure of an EUV mask (right) and defects in an EUV mask (left)

Cleaning processes should be able to remove contamination and particles from these surfaces but should not change their physical and chemical properties. In addition, chemical processes should not leave chemical residues, including molecular contamination, on the surface of the EUV mask.

Determining the critical defect size for an EUV mask is more complex than their so-called optical counterparts. EUV mask defects are a combination of EUV substrate, blank, and absorber patterning defects as is shown in Fig.1. During EUV mask blank fabrication, both particles and pit defects on the EUV substrate change when multilayers are deposited on the substrate. This change in defect size is commonly called defect decoration and depends on multilayer (ML) deposition conditions and the number of bilayers. In addition to substrate defects, particles are added by the multilayer deposition during the deposition (i.e., in-film particles) or after the deposition (top particles). Finally, defects are added during absorber layer deposition and patterning. A defect becomes a critical defect if it can print on the wafer. A few defect printability simulation studies [1] have predicted the dimension of a printable defect based on its size on the ML, its proximity to an absorber line, coherence of the EUV source, and the illumination angle and focus condition of the exposure tool. In addition to simulation studies, some recent works discuss experimental data on printable defect sizes on an EUV mask for certain nodes [2].

In this paper, we discuss those defects on top of the EUV mask when the mask is ready for exposure. Therefore, we will not address the cleaning processes required to manufacture EUV masks.

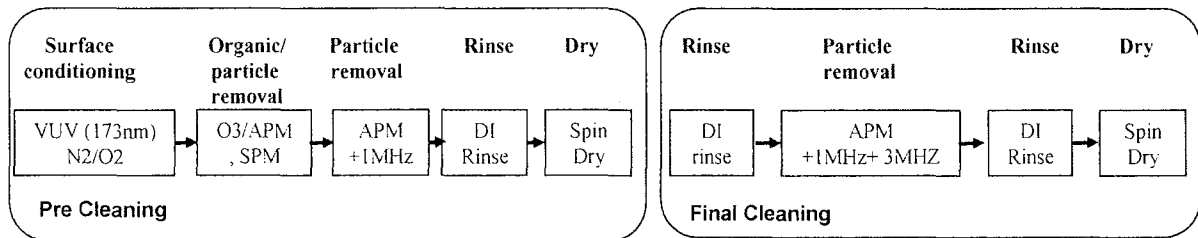


Figure 2- Typical cleaning process for EUV masks

Figure 2 is a diagram of a typical mask cleaning process. This process is divided into pre- and final cleaning. The cleaning process starts with a surface conditioning step in which the surface energy of the material is reduced in such way that the plate becomes hydrophilic and will be completely wet during subsequent wet processing steps. In the subsequent step, the plate will be rinsed and exposed to a strong oxidizer such as a (H_2SO_4/H_2O_2) mixture (i.e., SPM) or O_3 dissolved in water. SEMATECH has developed a similar process that uses an ($O_3/NH_4(OH)/H_2O_2/H_2O$) mixture (i.e., O_3/APM). During the organic removal steps, the pH of the solution is usually acidic and many particles are

deposited on the surface. Consequently, the particle removal step tends to follow the organic removal step. A $(\text{NH}_4\text{OH})/\text{H}_2\text{O}_2/\text{H}_2\text{O}$ mixture (APM) together with sonication is commonly used. SEMATECH uses a 1 MHz transducer in a nozzle configuration for particle removal. The next steps are a rinse and dry in which the remaining chemical will be rinsed and the surface spin-dried. SEMATECH uses a final cleaning process that is similar to pre-cleaning processes but in an acid-free environment, which usually cleans the surface better.

During the cleaning process, steps such as exposure to $\lambda=172$ nm UV light, sulfuric acid, ozone radicals, and sonication can change optical, chemical, and physical surface properties and, therefore, should be optimized properly.

2. EXPERIMENTS

Patterned EUV masks manufactured in Intel Corporation and Samsung were used for these experiments. The masks have line and space and elbow structures with a minimum 60 nm line width on mask and a pitch of 1:1 and higher. Ru-capped multilayer blanks with 40 and 50 bilayers of MoSi made at SEMATECH were used for particle removal and EUV reflectivity change and mask life time studies. Most of the cleaning experiments were done in a modified MaskTrack™ cleaning tool from Hamatech. SiO_2 particles with nominal diameters of 100 nm, 50 nm, and 28 nm and polystyrene latex (PSL) particles with a diameter of 20 nm were obtained from Microspheres-Nanospheres [3] and deposited manually from a solution by the droplet method. Plates then were dried by letting solvents evaporate under clean air. This method results in particles that are more difficult to remove compared to other deposition methods. SEM was used for pre- and post-cleaning inspection and calculating the local particle removal efficiency (PRE) of the cleaning process. EUV reflectivity measurements were done using an EUV reflectometer from EUV Technology [4] at SEMATECH.

SEMATECH's actinic inspection tool at Lawrence Berkeley National Lab (LBNL) was used to investigate the printability of deposited particles by EUV light ($\lambda=13.5$ nm).

Targeted megasonic experiments were performed in which the megasonic nozzle was positioned above a certain location on the mask and chemicals were dispensed during the megasonics application. During these experiments, the mask plate and nozzle were not moved with respect to each other. Megasonic power was controlled based on the maximum radio frequency (RF) power applied to the transducer. Maximum power applied to the megasonic transducer is about 35 W, which will result in power density of ~ 218 W/cm² near the transducer surface. Acoustic pressure measurements using fast hydrophones result in a maximum acoustic pressure of ~ 26 kPa at the surface of the transducer.

Fig. 3 shows a schematic of the nozzle configuration. A 1 MHz Sonosys [5] transducer was used for these experiments. The righthand graph shows the existing sub- and ultra-harmonics in the megasonic beam generated by a 1 MHz transducer from Sonosys.™ Note that although the resonant frequency is 1 MHz, the ultra-harmonics in this system go up to 12 MHz. Therefore, this system acts as a multimode megasonic system.

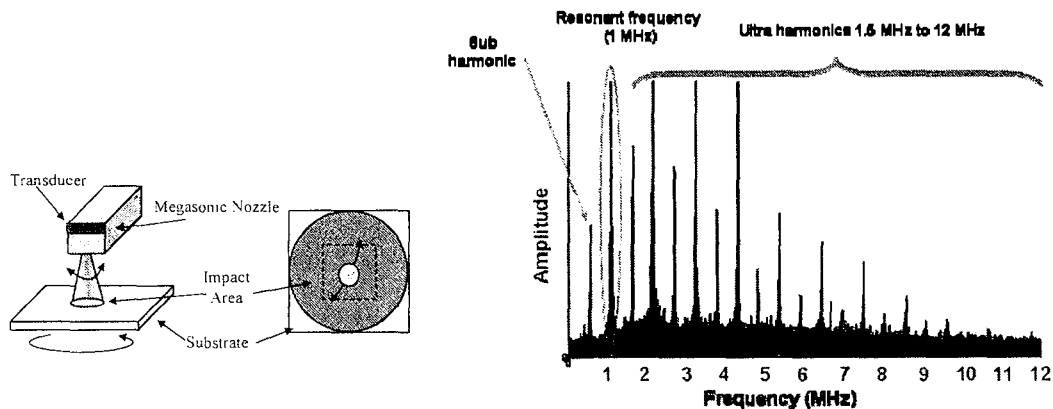


Figure 3- Typical nozzle megasonic configuration (left) and excited mode resulting from a 1 MHz transducer (right)

3. PARTICLE REMOVAL EFFICIENCY OF DEPOSITED PARTICLES

Cleaning processes should remove very small particles; however, these processes should not damage the patterned structures on the mask. The EUV masks used in these experiments had line patterns as small as 60 nm wide by a few microns long. This corresponds to the 15 nm HP node on the wafer (i.e., 4X magnification system). The pattern integrity was studied under both medium (87 W/cm^2) and high (174 W/cm^2) megasonic power.

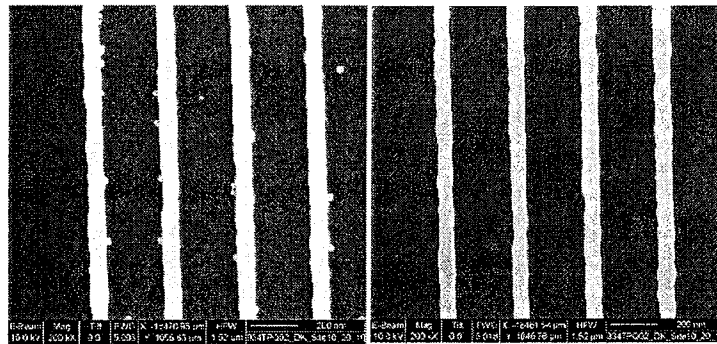


Figure 4 -SEM images of 60 nm TaBN lines on Ru-capped ML film before cleaning (left) and after cleaning (right).

Fig.4 shows 60 nm line patterns before and after cleaning with megasonic power (174 W/cm^2) for 5 min using the APM solution. As can be seen, the pattern lines suffer no apparent structural damage.

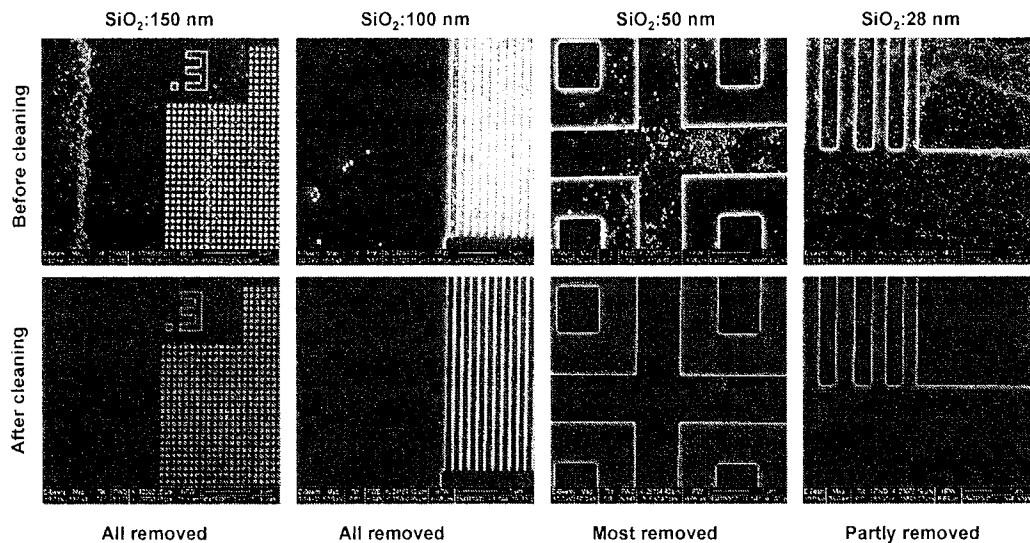


Figure 5- SEM images of different absorber patterned structures before cleaning (top row) and after cleaning (bottom row). Each column shows SiO₂ particles of different sizes were deposited on the surface. (Megasonic power: 174 W/cm^2 , APM chemistry)

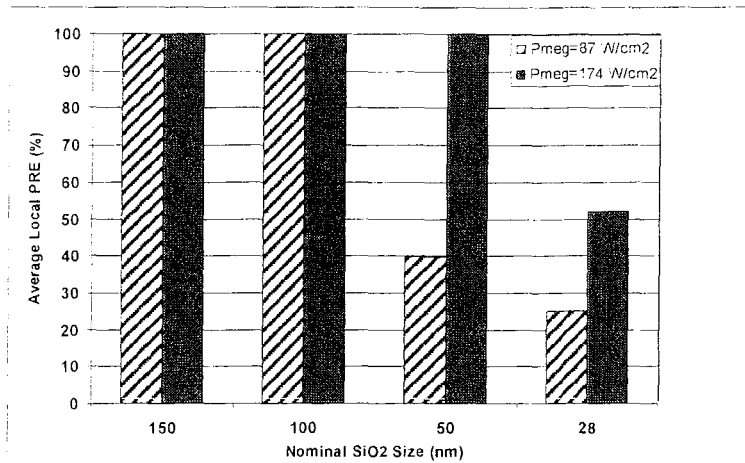


Figure 6- Average local PRE for different pattern structures vs. different SiO₂ particle sizes for two different applied megasonic powers.

Fig. 5 shows an example of particle removal for different pattern structures by megasonic cleaning with APM chemistry. Particles in each SEM image before and after cleaning were counted and the (local) PRE for each specific particle size was calculated. PREs were averaged by at least five SEM images for different pattern structures for each size of deposited SiO₂ particles. Results are plotted for two megasonic power levels in the Fig. 6.

PRE diminishes when particles become smaller due to the lower fluid velocity of small particles near the surface and their increased adhesion. As can be seen in Fig.6, increasing the megasonic power will increase PRE for all particle sizes. However, the PRE still remains about 50% for 28 nm SiO₂ particles. However, when a SPM process precedes the APM+ megasonic process, all 28 nm particles were removed from the trench patterns, as is shown in Fig. 7. The mechanism of particle removal by SPM is under investigation. SPM is a strong oxidizer and can dissolve most organic contamination. However, with silica particles, the SPM can not dissolve SiO₂. In addition, during a SPM process, the surface temperature rises up to 120°C due to an exothermic reaction between that sulfuric acid and hydrogen peroxide that are mixed at the point of use. Therefore, the combination of a higher temperature together with potential undercutting may undermine particle adhesion. Megasonic cavitation in the next step can then remove the particle from the surface.

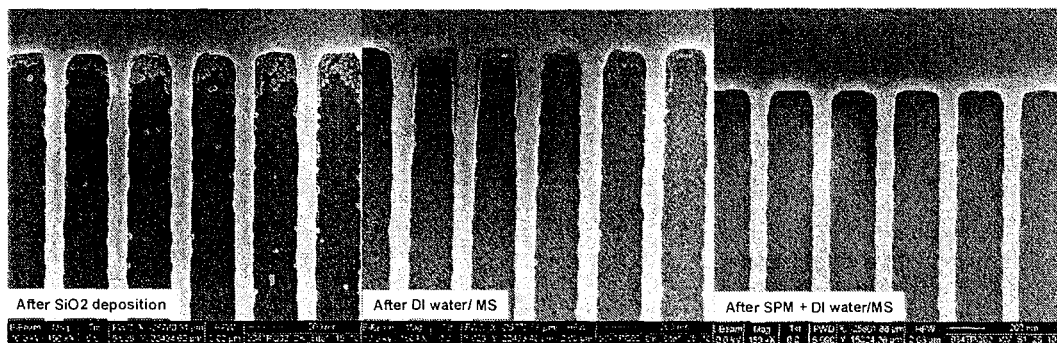


Figure 7- Deposited 28 nm SiO₂ particles inside trenches (left), after applying DI water and 1 MHz megasonic (middle). After applying SPM and DI water and 1 MHz megasonic (right).

After cleaning, the EUV reflectivity of this mask was measured. No change in EUV reflectivity was observed within the repeatability specification of our EUV reflectometer.

Particle removal efficiency depends on particle adhesion to the surface. Adhesion forces between the particle and surface result from van der Waals (vdW) interactions, electrostatic double-layer interactions, and short-range interactions. VdW forces depend on particle size, shape, distance from surface, and polarizability properties. Short-range (1-3 nm) interactions include solvation and other types of steric forces that are not considered here. Surface contributions are manifested in the electrostatic interaction. The surface energy can change depending on the history of the surface after its preparation. For example, exposure of the Ru cap to different etch plasmas and/or previous cleaning chemistries might increase or decrease Ru surface energy, which will increase or decrease the PRE. Hence, it is crucial to investigate how Ru surface treatment will affect PRE.

3.1 Effect of high current density SEM review on the PRE of defects

In addition to changes in the surface energy, the shape or adhesion properties of defect particles may change due to exposure to chemicals and radiation. Fig. 8 shows SEM images of SiO₂ particles deposited on a patterned structure in a 38 μm² area before cleaning (upper left image). A small 6 μm² area inside this image was scanned with higher magnification (50000X) with an e-beam (upper right image). As the e-beam current is fixed by reducing the scan area, current density increases by 40X. This mask was cleaned and then reviewed by SEM in both a large area (lower left) and small area (lower right) images. Comparison of large scanned areas before and after cleaning (left column) clearly demonstrates that the cleaning process has removed all particles with a PRE ~ 100%, except for the area that was exposed with a 40X higher current density.

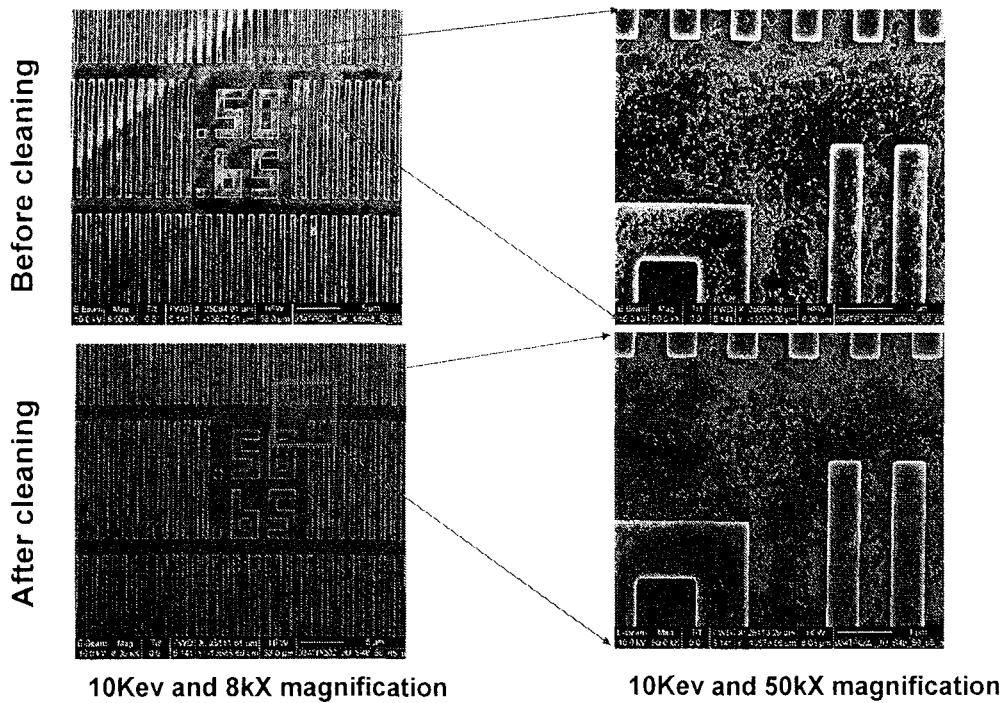


Figure 8 – Deposited 28 nm SiO₂ particles on an EUV pattern mask. Inspected with a 10 KeV SEM before and after cleaning a large area (38 μm²) (left column) and a small area (6 μm²) (right column)

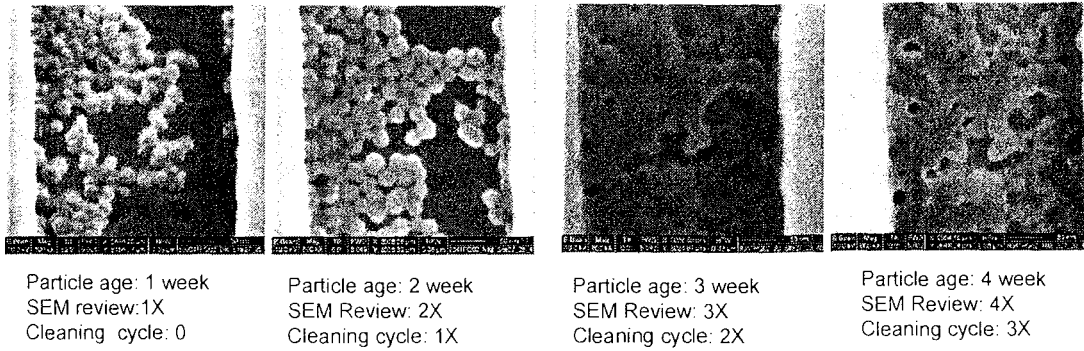


Figure 9 – Deposited 28 nm SiO₂ particles on an EUV pattern mask. Inspected with a 10 KeV SEM. Images from left to right show effect of defect age, cleaning cycle, and multiple SEM inspections

This effect becomes more pronounced when a patterned area undergoes multiple high current density SEM exposures. Fig. 9 shows the effect of combined defect aging, multiple cleanings, and multiple high current density SEM inspections on 28 nm SiO₂ particles. It is clear that 28 nm particles have not been removed by the cleaning and that particles have deformed and merged into each other to form a porous layer of SiO₂ instead of individual SiO₂ particles. Currently, experiments are in progress at SEMATECH to separate contribution of defect aging from defect deformation by high current density SEM inspection and review.

3.2 EUV mask lifetime as a function of mask cleaning

An EUV mask is expected to be used to expose about 50,000 wafers. During its lifetime and depending on different environmental and exposure conditions, an EUV mask may need to be cleaned up to 100 times. Therefore, the optical properties and the structure of the EUV mask should not be affected by cleaning process. In addition, cleaning processes should not contaminate the mask or add any particles to its surface.

To investigate EUV mask endurance under conventional cleaning processes, a series of experiments was performed on Ru-capped ML blanks. Fig. 10 shows the EUV reflectivity vs. cleaning cycles for three different cleaning processes: SPM, SEMATECH's O₃/APM, and APM (see Fig.2).

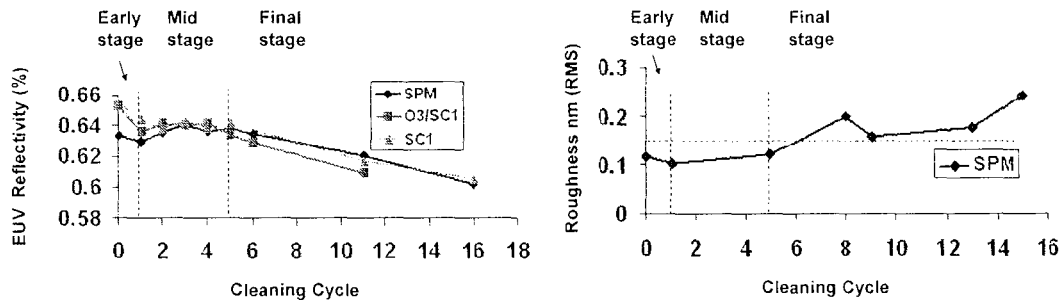


Figure 10 – EUV reflectivity of Ru-capped blanks as a function of the number of cleaning cycles for SPM, SEMATECH's O₃/APM, APM processes (left). Surface roughness as a function of cleaning cycle for the SPM process (right).

In general, the EUV reflectivity loss as a function of cleaning cycle can be divided into three stages: the early stage in which about 2% EUV reflectivity is lost after the first cleaning, the mid-stage that extends up to five cleaning cycles

during which EUV reflectivity does not change and is independent of the cleaning chemistry, and the final stage in which EUV reflectivity drops faster for ozonated chemistries than for SPM and APM processes.

As is shown in Fig. 10, EUV reflectivity reduces by about 6% after the blank is cleaned 16 times. Surface roughness remains unchanged until being cleaned 5 X, when it starts to increase in the final stage. Our investigation at SEMATECH has shown that the initial stage of EUV reflectivity reduction (i.e., 2% drop) results from Ru oxidation and depends on the method of Ru cap deposition. If Ru is deposited in the same chamber as the ML, then the Ru surface is not initially oxidized; however, if a separate chamber/method is used for Ru deposition, then the Ru will be oxidized. In mid-stage, the Ru surface is already oxidized and further oxidation will not change the EUV reflectivity. A sudden decrease in EUV reflectivity could be due to the removal of Ru by the cleaning process and deeper etching into ML.

TOFSIMS depth profiling was used to verify layer composition after cleaning with different chemistries. As shown in Fig. 2, the main steps in which active ozone radicals are generated are surface conditioning and O₃/APM. In the surface conditioning step, the Ru surface is exposed to VUV light with a wavelength of $\lambda = 178$ nm in a mixture of O₂ and N₂ gases. High energy 178 nm photons collide with O₂ molecules and create O₃⁻ radicals. In SEMATECH's O₃/APM process, O₃⁻ radicals are actively generated on the surface. In either case, the Ru surface is oxidized by exposure to O₃⁻ radicals.

Fig. 11 shows TOFSIMS depth profiles of a Ru-capped ML plate before cleaning. The top surface of the Ru is oxidized in its three stable oxidation valences (Ru⁺², Ru⁺⁴, Ru⁺⁶). However, the Ru oxide signal at the surface is 2X or 3X the Ru signal and it drops below the Ru signal about 2 nm from the top surface.

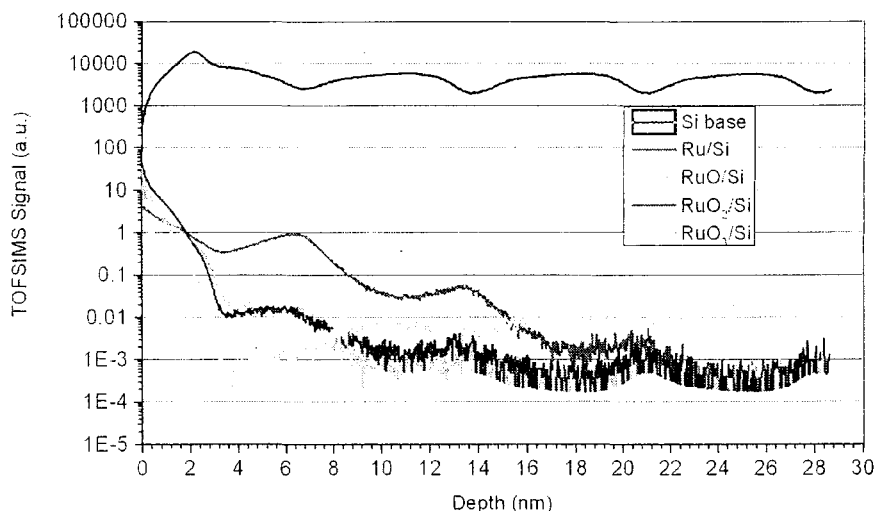


Figure 11 – TOFSIMS signals of the ratio of Ru oxides to Si for a Ru-capped ML plate. The Si base signal, which is used to determine different interfaces, is also shown.

Fig. 12 shows TOFSIMS depth profiles of a series of Ru-capped ML plates cleaned with different cleaning processes. (recipes A-G). These cleaning process are grouped into processes that use VUV (172 nm)+N₂ and those that use VUV (172 nm)+N₂/O₂. The TOFSIMS signal corresponding to the RuO of a non-cleaned plate (see Fig. 11) is also shown for comparison. After being cleaned 15 times, TOFSIMS signals of the Ru oxides in the VUV (172 nm)+N₂ processes have increased at the surface by about two orders of magnitude (~80X), indicating surface oxidation. However, all VUV (172 nm)+N₂/O₂ processes removed Ru on the top ~1.5 nm of the surface. Note that TOFSIMS signals for Ru oxides at this stage are not as high as when the process did not include oxygen. However, most of the Ru layer has been removed by ozone radicals and therefore not enough Ru remains to have high oxide signals.

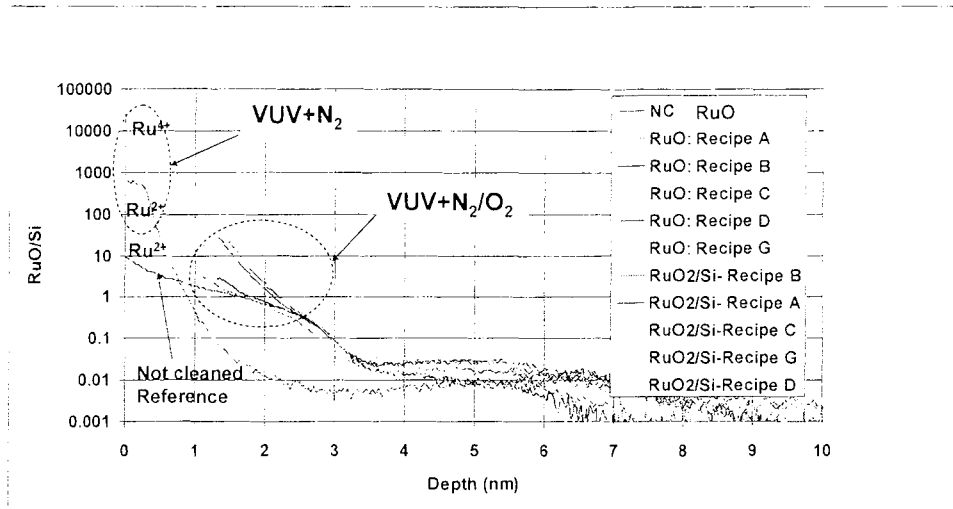


Figure 12 – TOF-SIMS signals of the ratio of Ru oxides to Si for plates cleaned with different cleaning processes (A-G) after 15 cleaning cycles. Ellipses show major differences in the surface conditioning of these cleaning processes

Fig.13 compares key performance parameters for newly developed cleaning processes that use VUV (172 nm)+N₂ (i.e., recipes D, E, F, G, H) with cleaning processes that use VUV (172 nm)+O₂/N₂ (i.e., recipes A, B, C). The details of the chemistries in these cleaning processes are different, which may lead to small variations among the different processes.

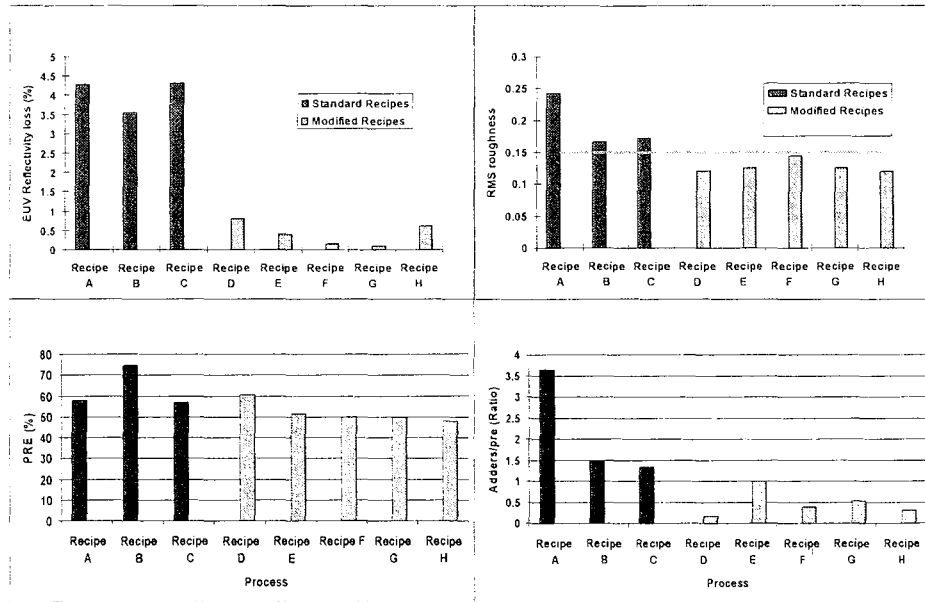


Figure 13 – EUV reflectivity loss (top left) and surface roughness (top right), PRE (bottom left), and ratio of added defects to the number of defects before cleaning (bottom right) after 5 cleaning cycles for cleaning process using VUV + O₂/N₂ (recipes A, B, C) and those using VUV + N₂ (recipes D, E, F, G, H).

However, the main contribution to all these processes comes from presence of O_3^* radicals. Newly developed cleaning processes outperform the O_2 -containing processes because they cause less EUV reflectivity loss. Lack of oxidation also causes less surface roughness after 15 cleaning cycles compared to cleaning processes with O_2 .

The PREs for newly developed cleaning processes are slightly lower but comparable with O_2 -containing processes, which is expected as O_3^* radicals have a high oxidation reduction power that contributes to particle removal; their absence in VUV+N₂ processes results in lower PREs. Finally, newly developed processes that do not use O_2 contribute fewer particle adders.

Therefore, got EUV masks with a Ru-capped ML, cleaning processes that use O_3^* radicals should be avoided to improve mask lifetime.

3.3 Printable defects on the top surface of an EUV mask

To optimize the particle removal capability of EUV mask cleaning processes, the sizes and composition of the particles that should be removed from the top surface of the mask must be determined. One reliable method is actinic ($\lambda=13.5$ nm) imaging of known defects on the surface. In a first attempt, 50 nm SiO₂ particles were deposited in the trenches of an EUV mask and were imaged by SEMATECH's EUV actinic inspection tool (AIT) at LBNL in Berkeley, CA. Due to current limitations in the imaging resolution of the AIT, larger size (50 nm) SiO₂ particles were chosen for this experiment. Note that optical properties (i.e., reflection, absorption, scattering) of defects and the surface at an EUV wavelength ($\lambda=13.5$ nm) together with tool-specific parameters will determine whether a specific defect will be imaged (i.e., will be printable on the wafer). SiO₂ particles were intentionally chosen as most of the cleaning process development was done using these particles. Fig. 14 shows two examples of SEM and actinic images of 50 nm SiO₂ particles inside 88 nm and 120 nm trenches, respectively. In the first SEM image, two SiO₂ particles at the end of the trench led to shortening of the line in the actinic image. In the second image, a single 50 nm SiO₂ particle inside the 120 nm trench appeared to have a smaller CD in the actinic image. Therefore, even though the current resolution of SEMATECH's AIT does not allow the imaging of sub-22 nm defects on top of multilayers, to the AIT can still provide valuable information about the size and composition of printable defects. Further experiments to investigate the printability of particles that have higher absorption than SiO₂ in the EUV wavelength (e.g., TaN) are planned..

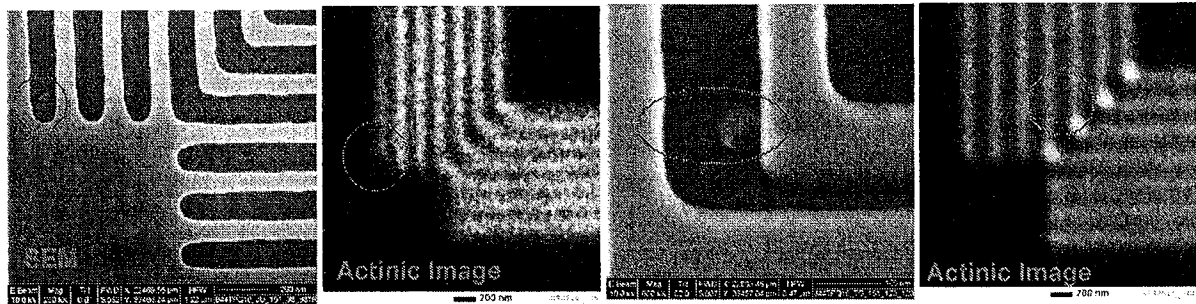


Figure 14 – SEM and actinic ($\lambda=13.5$ nm) images of two 50 nm SiO₂ particles at the end of a 88 nm trench (left); similar images of a single SiO₂ particle in a 120 nm trench (right). Actinic image shows a shortened line in the left image and smaller CD in the second image.

4. CONCLUSIONS

The PRE of cleaning processes diminishes when the minimum defect size for a specific technology node becomes smaller. For the sub-22 nm HP node, it was demonstrated that exposure to high power megasonics up to 200 W/cm² did

not damage 60 nm wide TaBN absorber lines, which correspond to the 16 nm HP node on the wafer. Furthermore, it was demonstrated the APM process with megasonics can remove ≥ 50 nm SiO₂ particles with very high PRE. Adding the SPM process to APM and high power (~ 175 W/cm²) megasonics is required to remove 28 nm SiO₂ particles with a high PRE.

TOFSIMS studies showed that O₂ in the VUV ($\lambda=172$ nm) surface conditioning step will both oxidize the surface and remove Ru, which drastically reduces EUV mask lifetime under multiple cleanings. When O₂ was removed from these cleaning processes, they caused negligible or no EUV reflectivity loss without increasing surface roughness up to 15 cleaning cycles.

Review of defects with a high current density SEM will drastically reduce PRE and deform SiO₂ particles. In addition, deposited 28 nm SiO₂ particles on EUV masks rapidly aged. Because SiO₂ particles commonly are used for calibrating short wavelength inspection tools, further studies are needed to confirm the size stability of these particles for inspection calibration or to find more suitable test particles.

ACKNOWLEDGEMENTS

The authors would like to acknowledge their colleagues in the metrology, inspection, cleaning sections of SEMATECH's Mask Blank Development Center (MBDC) for their support. Intel corp. and Samsung Electronics are acknowledged for providing EUV masks for these studies. Asahi Glass Co. is acknowledged for providing Ru-capped blanks for these experiments. Supported by the U.S. Department of Energy under Contract No. DE-AC02-05CH11231.

REFERENCES

1. Ch. H. Clifford *et al.*, "Investigation of buried EUV mask defect printability using actinic inspection and fast simulation," Proc. SPIE 7488,74882H (2009), See also latest Gullikson results in S. Huh, *et al.*, "Mask defect verification using actinic inspection and defect mitigation technology," Proc. SPIE 7271, 72713J (2009). See also the latest Terasawa results in T. Terasawa, *et al.*, "Development of actinic full-field EUV mask blank inspection tool at MIRAI-Selete," Proc. SPIE 7271, 727122 (2009).
2. R. Jonckheere *et al.*, "Investigation of EUV mask defectivity via full-field printing and inspection on wafer," Proc. SPIE 7379,73790R (2009), See also O. Wood, *et al.*, "Integration of EUV lithography in fabrication of 22 nm node devices," Proc. SPIE 7271,727104 (2009),
3. Microspheres-Nanospheres, Cold Spring, NY, USA
4. EUV Technology, Martinez, CA, USA
5. SONOSYS Ultraschallsysteme GmbH, Neuenbürg, Germany